

# Supporting Information

## Low-frequency Interlayer Breathing Modes in Few-layer Black Phosphorus

*Xi Ling<sup>†,¶,\*</sup>, Liangbo Liang<sup>‡,¶</sup>, Shengxi Huang<sup>†</sup>, Alexander A. Puretzky<sup>§</sup>, David B. Geohegan<sup>§</sup>,  
Bobby G. Sumpter<sup>§,‡</sup>, Jing Kong<sup>†</sup>, Vincent Meunier<sup>‡,\*</sup>, Mildred S. Dresselhaus<sup>†,‡,\*</sup>*

<sup>†</sup>Department of Electrical Engineering and Computer Science, Massachusetts Institute of Technology, Cambridge, Massachusetts 02139, USA.

<sup>‡</sup>Department of Physics, Applied Physics, and Astronomy, Rensselaer Polytechnic Institute, Troy, New York 12180, USA.

<sup>§</sup>Center for Nanophase Materials Sciences, Oak Ridge National Laboratory, Oak Ridge, Tennessee 37831, USA.

<sup>‡</sup>Computer Science and Mathematics Division, Oak Ridge National Laboratory, Oak Ridge, Tennessee 37831, USA.

<sup>†</sup>Department of Physics, Massachusetts Institute of Technology, Cambridge, Massachusetts 02139, USA.

<sup>¶</sup>These authors contributed equally to this work.

### **\* Correspondence Authors:**

**Prof. Mildred Dresselhaus**

**Department of Electrical Engineering and Computer Science,  
Massachusetts Institute of Technology, Cambridge, Massachusetts 02139, USA**

**Tel: +1-617-253-6864**

**Email: mdress@mit.edu**

**Prof. Vincent Meunier**

**Department of Physics, Applied Physics, and Astronomy,  
Rensselaer Polytechnic Institute, Troy, New York 12180, USA.**

**Tel: +1-518-276-6886**

**Email: meuniv@rpi.edu**

**Dr. Xi Ling**

**Department of Electrical Engineering and Computer Science,  
Massachusetts Institute of Technology, Cambridge, Massachusetts 02139, USA**

**Tel: +1-617-253-6860**

**Email: xiling@mit.edu**

**Content:**

**Section S1. Thickness-dependent interlayer breathing modes in BP**

**Section S2. Polarization dependence of Raman-active modes in BP**

**Section S3. High-frequency (HF) Raman spectra at different crystal rotation angles**

**Section S4. Thickness dependence of the HF Raman modes**

**Section S5. Temperature dependence of the Raman modes**

## Section S1. Thickness-dependent interlayer breathing modes in BP

**Table S1.** Calculated frequencies ( $\text{cm}^{-1}$ ) of interlayer breathing (B) modes for 2L and bulk BP based on different theoretical methods. The experimental frequency of the bulk B mode obtained using inelastic neutron scattering is also listed for comparison.<sup>1-4</sup> For the bulk, PBE+optB88 yields the best match with experimental frequency. PBE significantly underestimates the value, while other methods LDA, PBE+D2 and PBE+optB86b overestimate it. Thus, PBE+optB88 is adopted for our systematic study. More details about the calculation methods are provided in “Theoretical methods” of the main text.

	LDA	PBE	PBE+D2	PBE+optB86b	PBE+optB88	Experiment
2L	78.6	33.6	73.8	66.3	62.7	
bulk	105.5	46.6	103.3	91.3	86.1	87.1

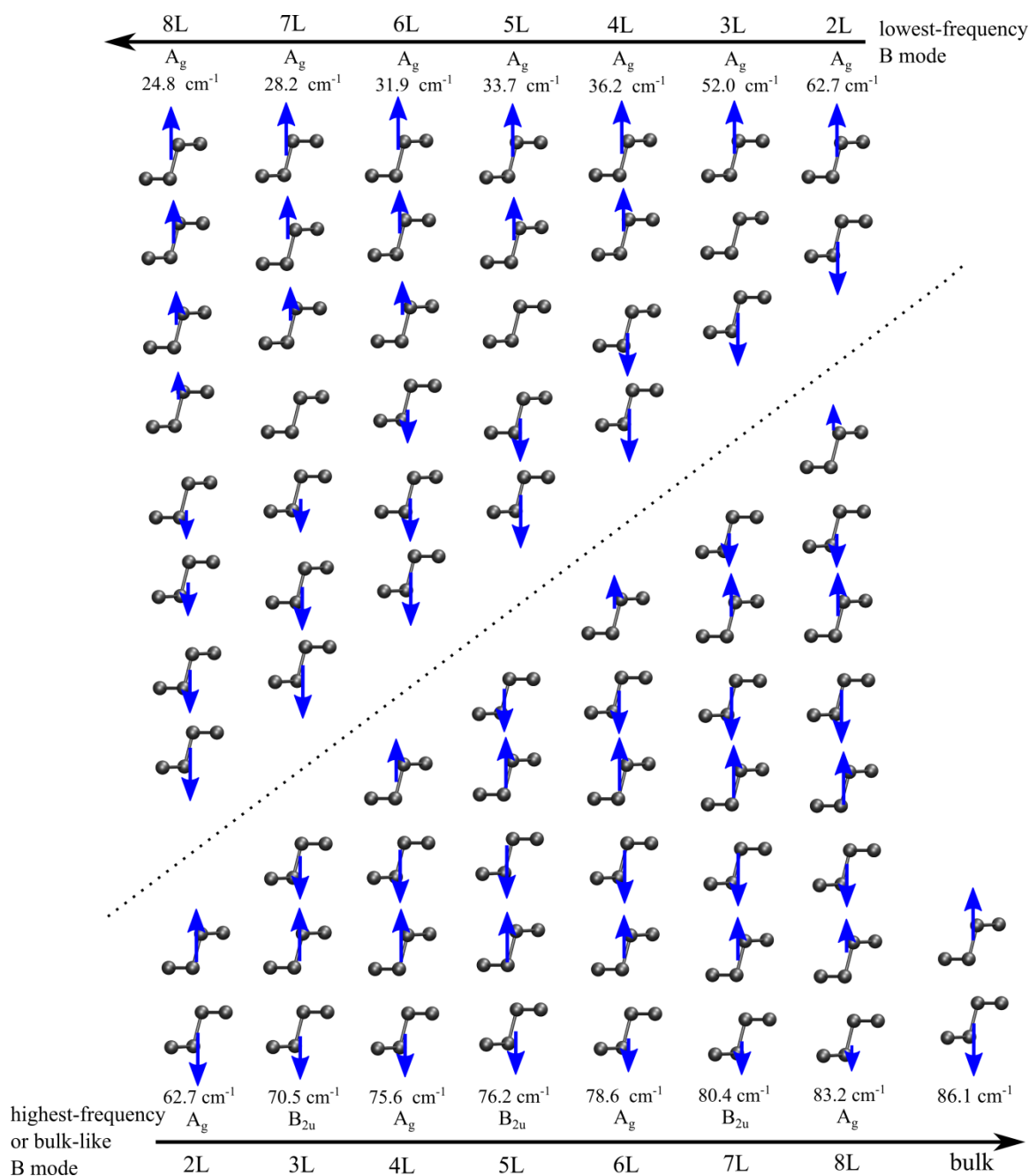


**Figure S1.** Calculated vibrations and frequencies of the highest-frequency and lowest-frequency B modes for 2L to 8L BP using PBE+optB88. Each blue arrow indicates the displacement of a whole layer. The highest-frequency B mode of any thickness is the bulk-like B mode, where each adjacent layer vibrates in opposite directions like the bulk. With increasing thickness, the highest frequency B mode blue shifts and approaches the bulk limit of  $\sim 87 \text{ cm}^{-1}$ . For the lowest-frequency B mode, generally, the top or bottom half segment shows in-phase displacements, and it is the two segments that vibrate in the opposite directions. Compared to the highest-frequency B mode, a greater proportion of in-phase displacements in the lowest-frequency B mode lead to lower frequencies. Note that for 2L, there is only one B mode (thus it is both the highest-frequency and lowest-frequency B mode).

## Section S2. Polarization dependence of Raman-active modes in BP

As mentioned in the main text, by denoting the X axis as the sample in-plane zigzag direction, the Y axis as the out-of-plane direction, and the Z axis as the in-plane armchair direction, the Raman tensors  $\tilde{R}$  of Raman-active modes  $A_g$ ,  $B_{1g}$ ,  $B_{2g}$  and  $B_{3g}$  are

$$\begin{aligned}\tilde{R}(A_g) &= \begin{pmatrix} a & \cdot & \cdot \\ \cdot & b & \cdot \\ \cdot & \cdot & c \end{pmatrix}, & \tilde{R}(B_{1g}) &= \begin{pmatrix} \cdot & d & \cdot \\ d & \cdot & \cdot \\ \cdot & \cdot & \cdot \end{pmatrix}, \\ \tilde{R}(B_{2g}) &= \begin{pmatrix} \cdot & \cdot & e \\ \cdot & \cdot & \cdot \\ e & \cdot & \cdot \end{pmatrix}, & \tilde{R}(B_{3g}) &= \begin{pmatrix} \cdot & \cdot & \cdot \\ \cdot & \cdot & f \\ \cdot & f & \cdot \end{pmatrix}.\end{aligned}\quad (S1)$$

In the typical experimental back-scattering laser geometry (Y in and Y out for the laser), the electric polarization vectors of the incident and scattered light  $e_i$  and  $e_s$  are in-plane (the X-Z plane). By setting the polarization angle of the incident (scattered) light as  $\theta$  ( $\gamma$ ) with respect to the X axis, we have  $e_i = (\cos\theta, 0, \sin\theta)$  and  $e_s = (\cos\gamma, 0, \sin\gamma)$ . Since the Raman intensity is  $I \propto |e_i \cdot \tilde{R} \cdot e_s^T|^2$ , we then have

$$I \propto \left| (\cos\theta, 0, \sin\theta) \tilde{R} \begin{pmatrix} \cos\gamma \\ 0 \\ \sin\gamma \end{pmatrix} \right|^2. \quad (S2)$$

Applying the Raman tensors  $\tilde{R}$  in Eq. S1 to Eq. S2, we can obtain the Raman intensities for each mode:

$$\begin{aligned}I_{A_g} &\propto a^2 \left| \cos\theta \cos\gamma + \frac{c}{a} \sin\theta \sin\gamma \right|^2, & I_{B_{2g}} &\propto e^2 \sin^2(\theta + \gamma), \\ I_{B_{1g}} &= 0, & I_{B_{3g}} &= 0.\end{aligned}\quad (S3)$$

Therefore,  $B_{1g}$  and  $B_{3g}$  cannot be observed, while only  $A_g$  and  $B_{2g}$  modes can be observed.

In general, there are two methods to study the polarization dependence. One is by rotating the sample while fixing the polarization of the incident and scattered light; the other is by changing the polarization of the incident or scattered light while fixing the sample. In this work, we have used the first method. The polarization angle of the incident and scattered light  $\theta$  and  $\gamma$  are fixed, and the sample is rotated in-plane (the X-Z plane) by  $\varphi$  with respect to the X axis. The rotation matrix and its inverse are

$$r = \begin{pmatrix} \cos\varphi & 0 & -\sin\varphi \\ 0 & 1 & 0 \\ \sin\varphi & 0 & \cos\varphi \end{pmatrix} \text{ and } r^{-1} = \begin{pmatrix} \cos\varphi & 0 & \sin\varphi \\ 0 & 1 & 0 \\ -\sin\varphi & 0 & \cos\varphi \end{pmatrix}. \quad (S4)$$

Consequently, for any Raman tensor  $\tilde{R}$ , the intensity becomes

$$\begin{aligned}
I &\propto \left| (\cos\theta, 0, \sin\theta) r \tilde{R} r^{-1} \begin{pmatrix} \cos\gamma \\ 0 \\ \sin\gamma \end{pmatrix} \right|^2 \\
&\propto \left| (\cos\theta, 0, \sin\theta) \begin{pmatrix} \cos\varphi & 0 & -\sin\varphi \\ 0 & 1 & 0 \\ \sin\varphi & 0 & \cos\varphi \end{pmatrix} \tilde{R} \begin{pmatrix} \cos\varphi & 0 & \sin\varphi \\ 0 & 1 & 0 \\ -\sin\varphi & 0 & \cos\varphi \end{pmatrix} \begin{pmatrix} \cos\gamma \\ 0 \\ \sin\gamma \end{pmatrix} \right|^2 \\
&\propto \left| (\cos\theta\cos\varphi + \sin\theta\sin\varphi, 0, -\cos\theta\sin\varphi + \sin\theta\cos\varphi) \tilde{R} \begin{pmatrix} \cos\varphi\cos\gamma + \sin\varphi\sin\gamma \\ 0 \\ -\sin\varphi\cos\gamma + \cos\varphi\sin\gamma \end{pmatrix} \right|^2 \\
&\propto \left| (\cos(\theta - \varphi), 0, \sin(\theta - \varphi)) \tilde{R} \begin{pmatrix} \cos(\gamma - \varphi) \\ 0 \\ \sin(\gamma - \varphi) \end{pmatrix} \right|^2. \tag{S5}
\end{aligned}$$

Compared to Eq. S2, we infer that the rotation of the crystal sample by  $\varphi$  is equivalent to rotation of the laser polarization of both the incident and scattered light by  $-\varphi$  with the sample fixed.

Under the parallel polarization configuration ( $\gamma = \theta$ ), based on Eq. S3 and Eq. S5, we then have

$$\begin{aligned}
I_{A_g} &\propto a^2 \left| \cos^2(\varphi - \theta) + \frac{c}{a} \sin^2(\varphi - \theta) \right|^2 \propto a^2 \left| 1 + \left(\frac{c}{a} - 1\right) \sin^2(\varphi - \theta) \right|^2, \\
I_{B_{2g}} &\propto e^2 \sin^2 2(\varphi - \theta), \\
I_{B_{1g}} &= 0, I_{B_{3g}} = 0. \tag{S6}
\end{aligned}$$

Since  $\theta$  is fixed, the intensity of an  $A_g$  mode depends on both the sample rotation angle  $\varphi$  and the ratio  $c/a$ , while the intensity of a  $B_{2g}$  mode only depends on the rotation angle  $\varphi$ . Clearly, the intensity variation period is always  $90^\circ$  for a  $B_{2g}$  mode: the intensity reaches the minimum at  $\varphi = \theta$  or  $\theta + 90^\circ$  or  $\theta + 180^\circ$  or  $\theta + 270^\circ$ , and the maximum at  $\varphi = \theta + 45^\circ$  or  $\theta + 135^\circ$  or  $\theta + 225^\circ$  or  $\theta + 315^\circ$ , as shown in Figure S2(b). For an  $A_g$  mode, the situation is more complicated due to the ratio  $c/a$ . If  $c/a = 1$  (i.e., isotropic), then  $I_{A_g} \propto a^2$  always, which has no dependence on the polarization (see Figure S2(a)). However, for anisotropic BP,  $c/a \neq 1$ . If  $c/a > 1$  (Figure S2(a)), the intensity variation period of an  $A_g$  mode is  $180^\circ$ , with the minimum intensity  $I_{A_g} \propto a^2$  at  $\varphi = \theta$  or  $\theta + 180^\circ$  (the sample is rotated by  $\theta$  and now the zigzag direction is along the

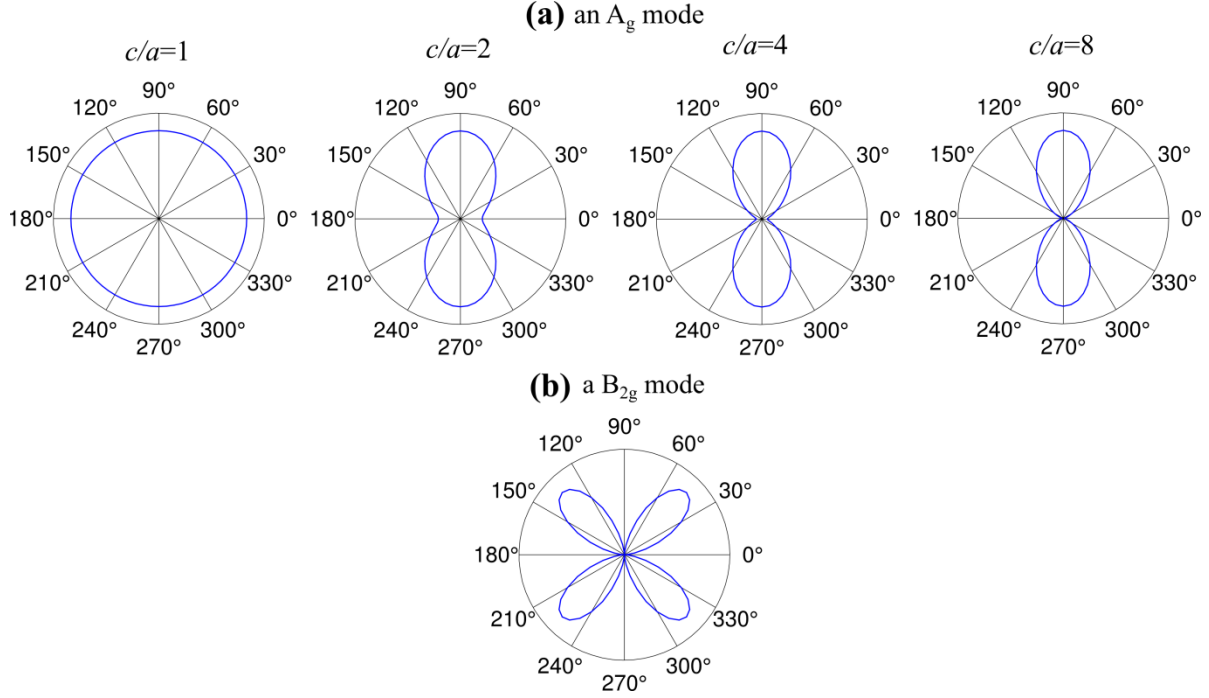


**Figure S2.** Theoretical polarization dependence by rotating the sample. Polar plots of calculated Raman intensities of (a)  $A_g$  and (b)  $B_{2g}$  modes as a function of crystal rotation angle  $\varphi$ . The polarization angle of the incident light  $\theta$  is set at  $0^\circ$  so that the sample initial zigzag direction is along the polarization direction of incident light. In (a), different  $c/a$  ratios are considered.

polarization direction of the incident light), and the maximum intensity  $I_{A_g} \propto c^2$  is at  $\varphi = \theta + 90^\circ$  or  $\theta + 270^\circ$  (the sample is rotated by  $\theta + 90^\circ$  and now the armchair direction is along the polarization direction of the incident light). If  $c/a < 1$ , the intensity variation period is still  $180^\circ$ , but the minimum and maximum intensity angles switch. According to our calculations and a previous experimental work for few-layer BP,<sup>5</sup> the value of  $c$  (Raman tensor component in the armchair direction) is expected to be larger than  $a$  (Raman tensor component in the zigzag direction), hence  $c/a > 1$ . In short, by rotating the crystal sample under a parallel polarization configuration, the intensity variation period is always  $180^\circ$  for an  $A_g$  mode, while it is always  $90^\circ$  for a  $B_{2g}$  mode. Additionally, when the sample armchair (zigzag) direction is along the polarization direction of the incident light, an  $A_g$  mode shows the maximum (minimum) intensity, while a  $B_{2g}$  mode is forbidden, as illustrated by the calculated polarization dependence of an  $A_g$  mode ( $c/a = 1, 2, 4, 8$ ) and an  $B_{2g}$  mode in Figure S2. In our calculations, the polarization angle of the incident light  $\theta$  is set at  $0^\circ$  so that the initial zigzag direction is along the polarization direction of the incident light before the sample rotation. Thus, the minimum and maximum

intensity rotation angles of an  $A_g$  mode are always  $0^\circ$  and  $90^\circ$ , respectively, in spite of the different ratios ( $c/a = 2, 4, 8$ ) in Figure S2(a). What is different is the quickly decreased minimum/maximum intensity ratio  $I_{min}/I_{max} \propto (a/c)^2$ . As a result, when  $c/a = 2$ , an  $A_g$  mode still shows relatively strong intensities at the minimum intensity rotation angle; when  $c/a = 8$ , an  $A_g$  mode is almost forbidden at the minimum intensity rotation angle. These results can explain the observed minor differences between the polarization dependence of the LF breathing modes and the HF  $A_g^1$  and  $A_g^2$  modes in Figures 3(b-g) of the main text.

Now we show how to determine the crystalline orientation of the BP flake based on its polarization dependence measured in Figure 3. According to Figures 3(b-g), after  $\sim 45^\circ$  clockwise rotation of the BP sample, the intensities of the  $A_g$  modes reach the maximum value and thus the sample armchair direction is now along the polarization direction of the incident light (i.e., the horizontal direction in the image of Figure 2(a)). Therefore, we conclude that before the rotation, the armchair direction of the sample is around  $45^\circ$  from the image in Figure 2(a).

Note that in the experimental back-scattering geometry, according to Eq. S3 and Eq. S6, the intensities of the  $B_{1g}$  and  $B_{3g}$  modes are zero under both methods, and thus their polarization dependence cannot be probed. If the BP sample is tilted out-of-plane instead of rotated in-plane, the  $B_{1g}$  and  $B_{2g}$  modes could be observed. From Eq. S1, Raman tensors for the  $B_{1g}$  and  $B_{3g}$  modes share similar formats to that of the  $B_{2g}$  mode (i.e., non-zero terms are all off-diagonal), indicating that their polarization dependence should be similar to the  $B_{2g}$  mode.

### Section S3. HF region of the Raman spectra at different crystal rotation angles

Figure S3 shows the HF region of the series of Raman spectra corresponding to Figure 3. When the sample is rotated by  $45^\circ$  and  $135^\circ$ , which are corresponding to the armchair and zigzag directions, respectively, the Raman intensity of the  $B_{2g}$  mode gets to the minima. The maxima intensity of  $A_g^1$  and  $A_g^2$  modes happens when the sample is rotated by  $45^\circ$  (the polarization of the incident light is along the armchair direction), and the minima intensity of  $A_g^1$  and  $A_g^2$  modes happens when the sample is rotated by  $135^\circ$  (the polarization of the incident light is along the zigzag direction),

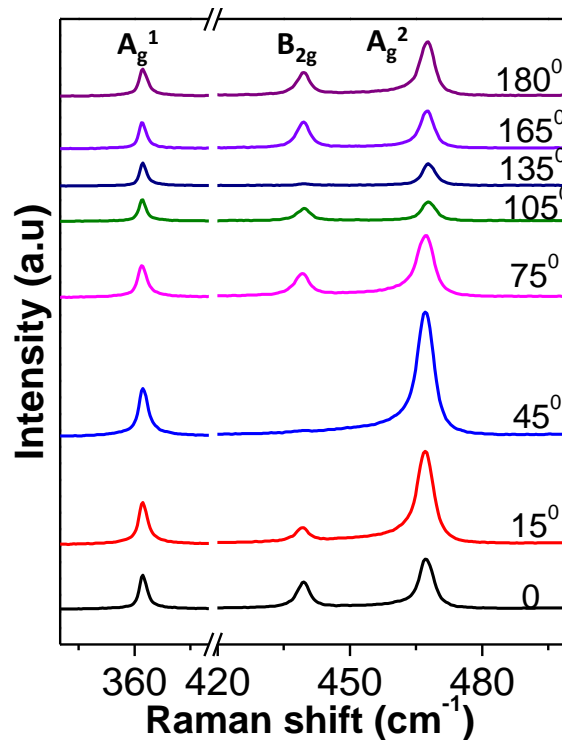


**Figure S3.** Experimental Raman spectra in the HF region of the few-layer BP (corresponding to Figure 2(a)) at the different rotation angles.

### Section S4. Thickness dependence of the HF Raman modes

Figure S4 shows the HF region of the Raman spectra of different BP flakes corresponding to the flakes in Figure 4. For flake 1-3, the intensities of the  $A_g^1$  and  $A_g^2$  modes are very weak. For flake 5, which is a little thicker, the intensities of the  $A_g^1$  and  $A_g^2$  modes are much stronger than that of flake 1-3. In addition, the frequency of the  $A_g^2$  mode red shifts obviously with the

increase of the thickness of the flakes. This strongly indicates that those flakes are very thin (less than 10 layers).

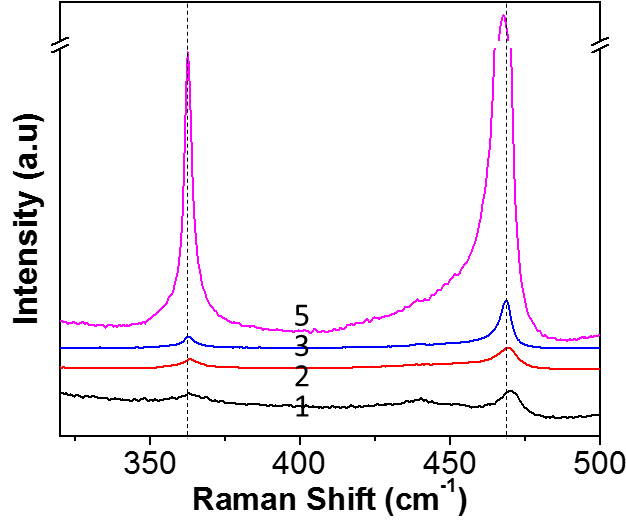
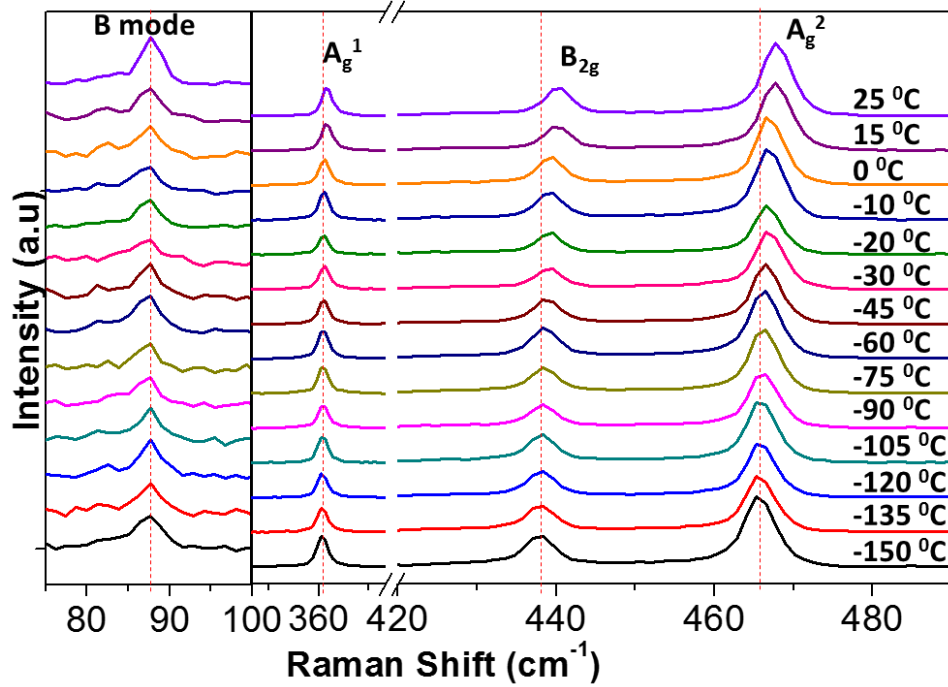


**Figure S4.** HF region of the Raman spectra of different BP flakes. The labels are corresponding to those in Figure 4.

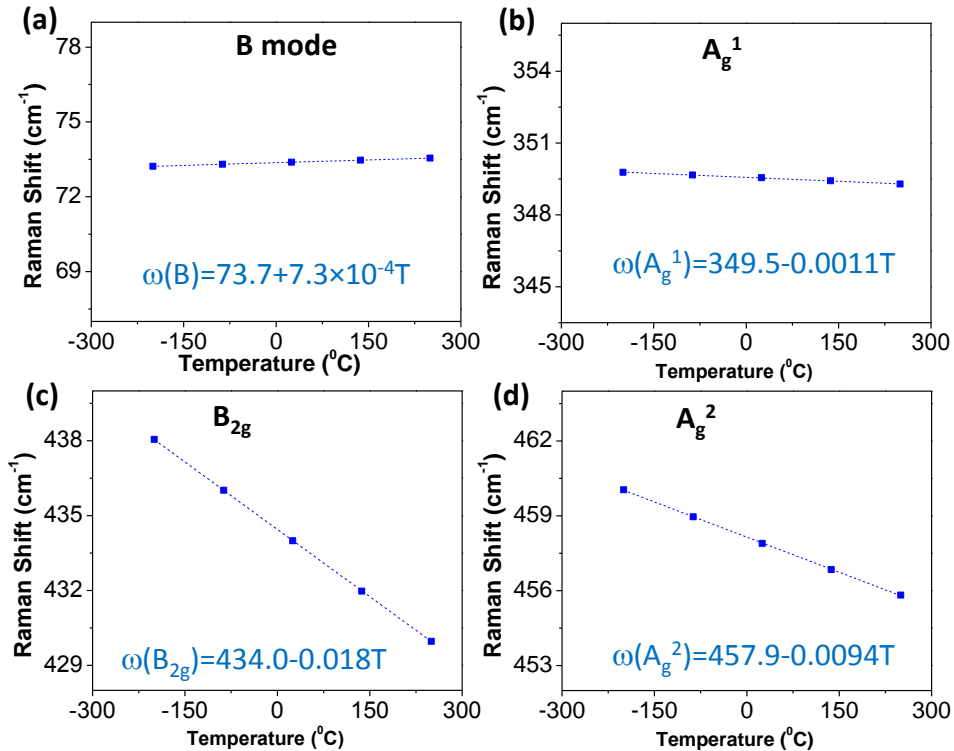
### Section S5. Temperature dependence of the Raman modes

Figure S5 shows the series of spectra corresponding to Figure 5. It is clear to see that the HF modes ( $A_g^1$ ,  $B_{2g}$  and  $A_g^2$ ) are obviously blue shifted with the increase of temperature from -150 °C to 25 °C, while the frequency of the B mode does not change too much. Considering the thermal expansion from both the crystal and the glass substrate, the temperature dependence of the B mode, and the  $A_g^1$ ,  $B_{2g}$  and  $A_g^2$  modes are calculated, as shown in Figure S6. For the B mode,  $B_{2g}$  and  $A_g^2$  modes, the temperature coefficients consistent with the experimental results. However, for  $A_g^1$  mode, the calculation result shows that this mode frequency does not have a strong dependence on the temperature, while the experimental result shows that the  $A_g^1$  blue shifts with the increase of the temperature. This result indicates that the thermal expansion is not the main contribution to the anharmonicity of the  $A_g^1$  mode. According to the temperature dependence of the frequency of the Raman mode:  $\omega = \omega_0 + \chi_T \Delta T + \chi_V \Delta V = \omega_0 + \left(\frac{\partial \omega}{\partial T}\right)_V \Delta T + \left(\frac{\partial \omega}{\partial V}\right)_T \Delta V$ , where the first term  $\left(\frac{\partial \omega}{\partial T}\right)_V \Delta T$  is the “self-energy” shift, which is the pure temperature

effect, and the second term  $(\frac{\partial\omega}{\partial V})_T\Delta V$  is due to the crystal thermal expansion. From this argument we conclude that the shift of the  $A_g^1$  frequency is mainly due to the “self-energy” shift.



**Figure S5.** Raman spectra of few-layer BP at different temperatures.



**Figure S6.** Calculated temperature dependence of the frequencies of the B mode (a), as well as of the  $A_g^1$  (b),  $B_{2g}$  (c), and  $A_g^2$  (d) modes.

### References

- (1) Fujii, Y.; Akahama, Y.; Endo, S.; Narita, S.; Yamada, Y.; Shirane, G. *Solid State Commun.* **1982**, *44* (5), 579–582.
- (2) Yamada, Y.; Fujii, Y.; Akahama, Y.; Endo, S.; Narita, S.; Axe, J.; McWhan, D. *Phys. Rev. B* **1984**, *30* (5), 2410–2413.
- (3) Jiang, J.-W.; Wang, B.-S.; Park, H. S. **2014**, arXiv:1412.7587.
- (4) Kaneta, C.; Katayama-Yoshida, H.; Morita, A. *J. Phys. Soc. Jpn.* **1986**, *55* (4), 1213–1223.
- (5) Wu, J.; Mao, N.; Xie, L.; Xu, H.; Zhang, J. *Angew. Chem.* **2015**, *127* (8), 2396–2399.